Dynamic Response and Wave Propagation in Plane Trusses and Frames

Y.-H. Pao, D.-C. Keh, S. M. Howard

Reprinted from

AIAA Journal

Volume 37, Number 5, Pages 594–603

AIAA

A publication of the
American Institute of Aeronautics and Astronautics, Inc.
1801 Alexander Bell Drive, Suite 500
Reston, VA 20191–4344

AIAA JOURNAL
Vol. 37, No. 5, May 1999

Dynamic Response and Wave Propagation in Plane Trusses and Frames

Yih-Hsing Pao* and Der-Ching Keh†
National Taiwan University, Taipei 106, Taiwan, Republic of China
and
Samuel M. Howard‡
Cornell University, Ithaca, New York 14853

The dynamics of planar frames and trusses is analyzed in terms of the propagation of axial (longitudinal) and flexural (transverse) stress waves being structural members. The waves are multiscattered at the joints, and scattering coefficients representing the reflection and transmission of both types of waves at each joint are derived from the dynamics and compatibility conditions of the joint. The complex multireflected waves within the structure are evaluated in the frequency domain by a newly developed reverberation matrix, which is formulated from scattering coefficients and propagating phase factors. Transient waves are then analyzed by Fourier synthesis and evaluated by a fast Fourier transform algorithm. Transient responses for the axial and bending strains in all structural members are calculated over a long duration for a model truss with rigid joints. Comparison to experimental data of the model truss under a step loading shows good agreement for the early as well as considerably long time responses.

I. Introduction

THE dynamic responses of framed structures, such as a truss or a rigid frame, have been traditionally analyzed by two approaches. One is to treat the structure as a multiconnected distributive system or continuous bodies of beams and columns, and the other is to discretize each and every structural member into finite numbers of elements (FEM).[1,2]

For the steady-state response of a distributive system, the stiffness matrix that relates the displacements of the joints to the forces in all connecting members is first derived. Because the forces and displacements at one end of a member are related to those at the other by the transfer matrix, the dynamic stiffness matrix (or compliance matrix) for all joints is then assembled for the entire structure.[3,4] Transient responses of the structure can then be calculated, in principle, by superposing the steady-state responses for all frequencies with the Fourier integral.[5]

For the discretized system the stiffness matrix for each element is estimated from the assumed shape functions for displacement and the mass. The mass matrix is estimated by averaging the kinetic energy with the assumed shape functions. A system of dynamic equations is then derived for the kinetic variables at all nodes of the discretized system.[6]

Recently, Nagem and Williams[7] proposed a new matrix formulation for planar structures. In their method the transfer matrices of all members are connected with joint coupling matrices to form the system matrix that characterized the steady-state response of the entire structure. Based on the system matrix, they have calculated the natural frequencies of a sample structure, and their results are more accurate than those determined from the dynamic compliance matrix or the finite element method.

In this paper we present an alternative matrix formulation for determining the dynamic response of distributive systems. This method, which was named as the method of reverberation matrix in a previous publication,[8] is particularly suitable for evaluating the transient response of a framed structure. In Ref. 8 the method was developed to analyze axial waves in a truss with rigid joints, and the results were compared to those developed by the ray-tracing method, which was presented earlier by Boley and Chao,[9] and to a set of carefully conducted experimental records.[10] Although the theoretical results agree very well with the experimental data for the early time response, they differ shortly after the initial period. As mentioned in Ref. 8, the divergence could be caused by neglecting the flexural waves at each joint. The reverberation matrix is thus modified in this paper by adding the modes of flexural waves in structural members.

In the modification the theory is improved by considering transverse displacement as well as axial displacement for all members. The propagation and scattering of three types of waves, the axial wave and the two modes of flexural waves based on the Timoshenko beam theory, are included in the newly formed reverberation matrix, from which the transient response of a structure is evaluated by applying the fast Fourier transform (FFT) algorithm.

We formulate in the next two sections scattering and reverberation matrices for the steady-state responses. In Sec. IV, we discuss the error that could be produced by applying the FFT algorithm. Section V presents the results for transient waves in three members of the model truss in Ref. 8 and the comparisons of the results obtained from the two theories as well as those from experiments. The accuracy of the present matrix formulation and calculation is ascertained by checking the balance of forces and moments for a considerably long time period. The paper ends with a brief conclusion in Sec. VII.

II. Motion of Structural Members and Joints

A frame structure is an assemblage of members (rods or beams) connected at joints with pins or rigid connectors. We identify joints by letters ($J, K, L, \ldots$) or numbers ($1, 2, \ldots$) and members by two letters or two numbers at both end joints ($IJ, JK, \ldots$; 1-2, 2-3, $\ldots$). For the truss illustrated in Fig. 1, there are 10 joints and 17 members. The joints, including those at supports, are identified by numbers 1–10 or $J, K, L, \ldots$, as shown. In this paper we indicate the total number by n, total number of members by m, and number of members meeting at the same joint J by m^J ($J = 1, 2, \ldots$). The total

Received April 10, 1997; revision received Oct. 23, 1998; accepted for publication Dec. 27, 1998.

*Professor, Institute of Applied Mechanics; on leave from Department of Theoretical and Applied Mechanics, Cornell University, Ithaca, NY 14853, Joseph C. Ford Professor.

†Graduate Assistant, Institute of Applied Mechanics; currently Assistant Professor, Division of Civil Engineering, Fushin Institute of Technology, Ilan 261, Taiwan, Republic of China.

‡Graduate Assistant, Department of Theoretical and Applied Mechanics; currently Senior Development Engineer, Vital Insite, Inc., 830 Dubuque Avenue, San Francisco, CA 94080.

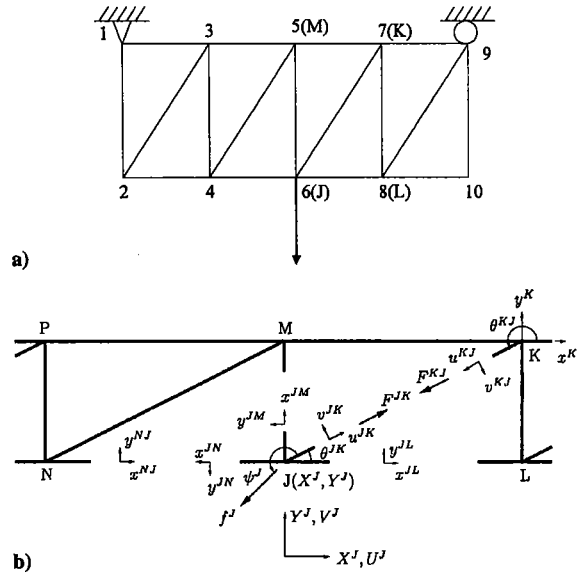

Fig. 1 Geometry of a planar model truss: a) labeling of 10 joints and 17 structural members and b) forces and moments at the joints in local and global coordinates.

number of structural members m is related to the sum of numbers m^J $(J = 1, 2, \ldots, n)$ and

$$\sum_{J=1}^{n} m^J = 2m$$

All joints on a plane are referred to common Cartesian coordinates $(X, Y, Z = 0)$, which are called the global coordinates of the structure. For each member JK, we introduce two right-hand systems of coordinates, $(x, y)^{JK}$ with origin at J and $(x, y)^{KJ}$ at K; the directions of x^{JK} and y^{JK} are opposite to those of x^{KJ} and y^{KJ}, respectively. We call $(x, y)^{JK}$ and so on the local coordinate systems.

The components of any physical quantities in the structure may be expressed either in global coordinates or in local coordinates. Denote the two components of the vector $\boldsymbol{v}$ in local coordinates by v_i $(i = x, y)$ and those in global coordinates by the transformation matrix $\boldsymbol{T}_{iK}$:

$$v_i = \sum T_{iK} v_K \tag{1}$$

For the member JK shown in Fig. 1, $T_{xX} = \cos\theta$, $T_{xY} = \sin\theta$, $T_{yX} = -\sin\theta$, and $T_{yY} = -\cos\theta$.

In terms of the local coordinates, there are two components for the displacement vector in each structural member, the axial displacement $u(x, t)$ along the x axis and the transverse displacement $v(x, t)$ in the direction of the y axis: the latter is decomposed further into two parts, $v_s(x, t)$ due to shear and $v_b(x, t)$ due to bending. In addition, there is the rotation of the cross section about the z axis, $\phi = dv_b/dx$. Corresponding to the three displacement components (u, v, ϕ), there are two resultant forces and one moment: the axial force $F(x, t)$, shear force $V(x, t)$, and bending moment $M(x, t)$, all acting through the centroid of each cross section.

The sign conventions for the physical quantities are defined as follows: u, v_b, and v_s are positive if they point into the positive direction of the x or y axis; F, V, and M are positive if they act on a plane with positive (or negative) outer normal and point or relate to a positive (or negative) axis. Because each cross section of a member JK is viewed from two sides, one in the direction of x^{JK} and the other in the direction of x^{KJ} $(l^{JK} - x^{JK})$, we have

$$(u^{JK}, V^{JK}, \phi^{JK}) = (-F^{KJ}, -V^{KJ}, \phi^{KJ}) \tag{2}$$

$$(F^{JK}, V^{JK}, M^{JK}) = (-F^{KJ}, -V^{KJ}, -M^{KJ}) \tag{3}$$

A. Axial and Flexural Waves in Structural Members

We assume that the cross-sectional area and material properties for each structural member are constant throughout the length between two joints. The area A, section moment of area I, mass density ρ, Young's modulus, and shear modulus G, however, may be different from member to member.

For each member (superscript omitted) the axial displacement $u(x, t)$ satisfies the wave equation, and the axial force $F(x, t)$ equals $EA\partial u/\partial x$.

Denote the Fourier transform of a physical variable with respect to t by an overhead caret; for example,

$$\hat{u}(x, \omega) = \int_{-\infty}^{\infty} u(x, t)\, e^{-i\omega t}\, dt \tag{4a}$$

The inverse transform of $\hat{u}(x, t)$ is given by

$$u(x, t) = \frac{1}{2\pi} \int_{-\infty}^{\infty} \hat{u}(x, t)\, e^{i\omega t}\, dt \tag{4b}$$

The Fourier-transformed wave equation is

$$\frac{d^2\hat{u}}{dx^2} + \frac{\omega^2}{c_1^2}\hat{u} = 0 \tag{5a}$$

where $c_1^2 = E/\rho$. The Fourier-transformed axial force is thus given by

$$\hat{F} = EA\frac{d\hat{u}}{dx} \tag{5b}$$

The solutions for $\hat{u}(x, \omega)$ and $\hat{F}(x, \omega)$ are

$$\hat{u}(x, \omega) = a_1(\omega)\, e^{ik_1 x} + d_1(\omega)\, e^{-ik_1 x} \tag{6a}$$

$$\hat{F}(x, \omega) = EAik_1\left[a_1 e^{ik_1 x} - d_1 e^{-ik_1 x}\right] \tag{6b}$$

where $k_1 = \omega/c_1$ and $a_1(\omega)$ and $d_1(\omega)$ are the unspecified amplitudes. With reference to the joint J at $x^{JK} = 0$ and the time vector $\exp(i\omega t)$, we call a_1 the arriving wave amplitude and d_1 the departing wave amplitude.

The flexural wave in each member is governed by Timoshenko's theory of beams.[11] We decompose the transverse displacement into v_b and v_s and express the deflection of the centerline by v and the rotation of the cross section by ϕ, $v = v_b + v_s$, $\phi = \partial v_b/\partial x$. The Fourier-transformed equations of motion $\hat{v}_b(x, \omega)$ and $\hat{v}_s(x, \omega)$ are

$$EI\frac{d^3\hat{v}_b}{dx^3} + \kappa AG\frac{d\hat{v}_s}{dx} = -\rho I\omega^2\frac{d\hat{v}_b}{dx} \tag{7a}$$

$$\kappa AG\frac{d^2\hat{v}_s}{dx^2} = -\rho A\omega^2(\hat{v}_b + \hat{v}_s) \tag{7b}$$

where κ is the shear coefficient of the member, which is assumed to be $\pi^2/12$ in this paper. The transformed angle of rotation $\hat{\phi}$, any moment $\hat{M}$, and shear force $\hat{V}$ are given, respectively, by

$$\hat{\phi}(x, \omega) = \frac{d\hat{v}_b}{dx}, \qquad \hat{v}(x, \omega) = \kappa AG\frac{d\hat{v}_s}{dx}$$
$$\hat{M}(x, \omega) = EI\frac{d^2\hat{v}_b}{dx^2} \tag{8}$$

The solutions of Timoshenko's beam equation (8) are

$$\hat{v}_b(x, \omega) = a_2(\omega)\, e^{ik_2 x} + d_2(\omega)\, e^{-ik_2 x} + a_3(\omega)\, e^{ik_3 x} + d_3(\omega)\, e^{-ik_3 x} \tag{9a}$$

$$\hat{v}_s(x, \omega) = \alpha_2 a_2(\omega)\, e^{ik_2 x} + \alpha_2 d_2(\omega)\, e^{-ik_2 x} + \alpha_3 a_3(\omega)\, e^{ik_3 x} + \alpha_3 d_3(\omega)\, e^{-ik_3 x} \tag{9b}$$

where $a_2(\omega)$, $a_3(\omega)$, $d_2(\omega)$, and $d_3(\omega)$ are unspecified amplitudes of arriving waves and departing waves, respectively. The wave members k_2, k_3 are related to ω by

$$k_{2,3}(\omega) = \sqrt{1 + \eta \pm \sqrt{(1+\eta)^2 - 4\left[\eta - \frac{c_1^2}{(R\omega)^2}\right]}} \Bigg/ \sqrt{2}c_1 \tag{10}$$

where $\eta = E/KG$ and $c_s = \sqrt{(G/\rho)}$. Corresponding to each k, the ratio of v_b and v_s is

$$\alpha_{2,3}(\omega) = R^2 \frac{\omega^2 - c_2^1 k_{2,3}^2}{\kappa c_s^2}$$

The speeds of the flexural waves are dispersive; the wave speeds are $c_{2,3} = \omega/k_{2,3}$. One of the two waves may be nonpropagating if k_3 is imaginary. The solutions for $\hat{\phi}$, $\hat{M}$, $\hat{V}$ are calculated from $\hat{v}_b$ and $\hat{v}_s$ according to Eq. (8).

B. Equations of Motion and Compatibility Conditions at a Free or Supported Joint

We denote external forces and moments applied at joint J by f_X^J, f_Y^J, and μ^J $(J = 1, 2, \ldots, n)$, respectively. The displacement field of joint J is composed of $U^J(t)$, $V^J(t)$ in the direction of the X axis and Y axis, respectively, and a rotation $\Phi^J(t)$ about the Z axis. Under the action of external forces, the motion of the joint J is constrained by the internal forces F^{JK}, V^{JK}, and the internal bending moment M^{Jk} $(k = 1, 2, \ldots, m^J)$ in all members.

Applying Newton's law to a moving joint with a concentrated mass M^J, we obtain three equations of motion, which in the Fourier-transformed domain take the forms

$$\sum_{k=1}^{m^J} [\hat{F}^{JK}(0, \omega) \cos\theta^{JK} - \hat{V}^{JK}(0, \omega) \sin\theta^{JK}] + \hat{f}_X^J = -\omega^2 M^J \hat{U}^J \tag{11a}$$

$$\sum_{k=1}^{m^J} [\hat{F}^{JK}(0, \omega) \sin\theta^{JK} - \hat{V}^{JK}(0, \omega) \cos\theta^{JK}] + \hat{f}_Y^J = -\omega^2 M^J \hat{V}^J \tag{11b}$$

$$\sum_{k=1}^{m^J} \hat{M}^{JK}(0, \omega) + \hat{\mu}^J = -\omega^2 M^J \gamma^2 \hat{\Phi}^J \tag{11c}$$

where γ is the radius of gyration of joint J about the Z axis. The transformed forces and moments in members acting at J can be expressed in terms of the arriving and departing wave amplitudes at each member, according to Eqs. (6), (8), (9a), and (9b) for $x = 0$. The number of unknowns by this substitution is then increased to $6m^J$.

The displacements and angular rotation at the end of each member should be compatible with those of the connecting joint. If all members are rigidly connected at the joint, they must satisfy the following compatibility equations for $k = 1, 2, \ldots, m^J$ at each joint:

$$\hat{u}^{Jk}(0, \omega) \cos\theta^{Jk} - \hat{v}^{Jk}(0, \omega) \sin\theta^{Jk} = \hat{U}^J(\omega) \tag{12a}$$

$$\hat{u}^{Jk}(0, \omega) \sin\theta^{Jk} - \hat{v}^{Jk}(0, \omega) \cos\theta^{Jk} = \hat{V}^J(\omega) \tag{12b}$$

$$\hat{\phi}^{Jk}(0, \omega) = \hat{\Phi}^J(\omega) \tag{12c}$$

If all members are pin-connected at the joint, we replace Eq. (12c) by the conditions of free rotation or the conditions of vanishing moment:

$$M^{Jk}(0, \omega) = 0 \qquad (k = 1, 2, \ldots, m^J) \tag{12d}$$

In either case the conditions of compatibility for m^J members at each joint thus supply $3m^J$ additional equations.

The two sets of Eqs. (11) and (12) form a system of $3(m^J + 1)$ equations containing $6m^J$ unknown amplitudes a_i^{Jk} and d_i^{Jk} $(i = 1, 2, 3)$ and a total of six components for the force and displacement at a joint.

Of the six components for the state vector of force at a joint $\{\hat{f}_X^J, \hat{f}_Y^J, \hat{\mu}^J\}$ and that of displacement $\{\hat{U}^J, \hat{V}^J, \hat{\Phi}^J\}$ in Eqs. (11) and (12), only three of them are unknown quantities, depending on the support conditions at each joint as described in the following:

1) Free joint with external force: The $\hat{f}_X^J$, $\hat{f}_Y^J$, and $\hat{\mu}^J$ are prescribed, whereas $\hat{U}^J$, $\hat{V}^J$, and $\hat{\Phi}^J$ are unknowns. Furthermore, if all members are pin-connected at the joint, $\hat{M}^{Jk}$ in Eq. (11c) vanishes.

2) A joint welded to a moving support: The $\hat{U}^J$, $\hat{V}^J$, and $\hat{\Phi}^J$ are prescribed, whereas $\hat{f}_X^J$, $\hat{f}_Y^J$, and $\hat{\mu}^J$ are unknowns.

3) A joint hinged to a moving support: The $\hat{U}^J$, $\hat{V}^J$, and $\hat{\mu}^J$ are prescribed, whereas $\hat{f}_X^J$, $\hat{f}_Y^J$, and $\hat{\Phi}^J$ are unknowns.

4) A joint hinged to a sliding support (free sliding along X axis): The $\hat{f}_X^J$, $\hat{V}^J$, and $\hat{\mu}^J$ are prescribed, whereas $\hat{U}^J$, $\hat{f}_Y^J$, and $\hat{\Phi}^J$ are unknowns.

Therefore, we have established a system of $3(m^J + 1)$ equations for a total of $6m^J + 3$ unknowns in Eqs. (11) and (12).

III. Scattering and Reverberation Matrix for the Structure

In the preceding set of Eqs. (11) and (12), we can solve for $3m^J$ unknown amplitudes d_i^{JK} by treating a_i^{JK} and the forces or displacements at the joint as given quantities, thereby establishing the local scattering matrix at each and every joint. The local scattering matrices are then stacked up to form the global scattering matrix for the entire structure, which relates the departing wave vector $\boldsymbol{d}$ to the arriving wave vector $\boldsymbol{a}$ in matrix form. Another set of equations relating $\boldsymbol{d}$ to $\boldsymbol{a}$ is obtained through the phase relations between the arriving and departing waves. All of the unknown coefficients $\boldsymbol{a}$ and $\boldsymbol{d}$ are thus determined from the external forces in terms of the reverberation matrix, which is the product of scattering matrix, phase matrix, and permutation matrix. Details of the derivation are given in the next two subsections.

A. Scattering Matrix

To derive the local scattering matrix as well as the source vector from Eqs. (11) and (12), we can consider the motion of a free joint $\boldsymbol{J}$ with neighboring joints $\boldsymbol{K}, \boldsymbol{L}, \boldsymbol{M}, \boldsymbol{N}$, as shown in Fig. 1b. The departing amplitudes d_i^{Jq} $(q = K, L, M, N; i = 1, 2, 3)$ are then solved in terms of a_i^{Jp} and the external forces. The results are expressed as

$$\boldsymbol{d}_i^{Jq} = \sum_{p=K}^{N} \sum_{j=1}^{3} \boldsymbol{S}_{ij}^{qJp} \boldsymbol{a}_j^{Jp} + \boldsymbol{s}_i^{Jq} \tag{13a}$$

where S_{ij}^{qJp} are scattering coefficients for waves from joint $\boldsymbol{p}$ through $\boldsymbol{J}$ to the joint $\boldsymbol{q}$ with mode conversion j to i. The source vectors $\boldsymbol{s}_i^{Jq}$ represent the departing waves in member $\boldsymbol{Jq}$ generated by the force $\boldsymbol{f}^J$, and they could be determined directly by solving Eqs. (11) and (12) with $a_i^{Jp} = 0$.

Equation (13a) may be expressed in matrix form:

$$\boldsymbol{d}_i^{Jq} = \sum_{p=K}^{N} \boldsymbol{S}^{qJp} \boldsymbol{a}^{Jp} + \boldsymbol{s}^{Jq} \qquad (q = K, L, M, N) \tag{13b}$$

For convenience, we call the column matrix $\boldsymbol{a}^{Jp}$ the *arriving wave vector* in member $\boldsymbol{Jp}$ and $\boldsymbol{d}^{Jq}$ the *departing wave vector* in member $\boldsymbol{Jp}$, despite the fact that neither one of them is a true vector in three-dimensional space.

The four column matrices of $\boldsymbol{d}^{Jq}$ may be stacked in a single-column matrix as follows:

$$\begin{Bmatrix} \boldsymbol{d}^{JK} \\ \boldsymbol{d}^{JL} \\ \boldsymbol{d}^{JM} \\ \boldsymbol{d}^{JN} \end{Bmatrix} = \begin{bmatrix} \boldsymbol{S}^{KJK} & \boldsymbol{S}^{KJL} & \boldsymbol{S}^{KJM} & \boldsymbol{S}^{KJN} \\ \boldsymbol{S}^{LJK} & \boldsymbol{S}^{LJL} & \boldsymbol{S}^{LJM} & \boldsymbol{S}^{LJN} \\ \boldsymbol{S}^{MJK} & \boldsymbol{S}^{MJL} & \boldsymbol{S}^{MJM} & \boldsymbol{S}^{MJN} \\ \boldsymbol{S}^{NJK} & \boldsymbol{S}^{NJL} & \boldsymbol{S}^{NJM} & \boldsymbol{S}^{NJN} \end{bmatrix} \begin{Bmatrix} \boldsymbol{a}^{JK} \\ \boldsymbol{a}^{JL} \\ \boldsymbol{a}^{JM} \\ \boldsymbol{a}^{JN} \end{Bmatrix} + \begin{Bmatrix} \boldsymbol{s}^{JK} \\ \boldsymbol{s}^{JL} \\ \boldsymbol{s}^{JM} \\ \boldsymbol{s}^{JN} \end{Bmatrix} \tag{14}$$

where each vector $\boldsymbol{d}^{JK}$, etc., is composed of three components $(d_1^{JK}, d_2^{JK}, d_3^{JK})$, etc., and $\boldsymbol{S}^{KJK}$, $\boldsymbol{S}^{KJL}$, and so on are 3×3 submatrices.

The matrix equation (14) is further simplified in notation as

$$\boldsymbol{d}^J = \boldsymbol{S}^J \boldsymbol{a}^J + \boldsymbol{s}^J \tag{15}$$

where $\boldsymbol{S}^J$ $(3m^J \times 3m^J)$ is called the *local scattering matrix* at joint $\boldsymbol{J}$, and $\boldsymbol{s}^J$ $(3m^J \times 1)$ is called the *local source vector* at that joint. The local scattering matrix is the solution of Eqs. (11) and (12) that relates the local departing wave vector $\boldsymbol{d}^J$ to the local arriving wave vector $\boldsymbol{a}^J$ at the joint $\boldsymbol{J}$. It might be different from joint to joint, depending on the neighboring members and the support conditions in the preceding sections.

For example, if the hinged support is fixed, Eqs. (13) are then determined from the condition U^J, V^J, and $\mu^J = 0$. The reactive

forces f_X^J and f_Y^J and rotation Φ^J at the hinged support can then be calculated from Eqs. (11) and (12). On the other hand, if the hinged joint is supported by a roller free to slide in the X direction, then the vertical reactive forces f_Y^J, displacement U^J, and rotation Φ^J are treated as unknowns; the scattering matrix is then solved by eliminating these variables from the system of Eqs. (11) and (12) with the condition $f_X^J = 0$, $V^J = 0$, and $\mu^J = 0$.

Assembling all departing wave vectors $\boldsymbol{d}^J$ for all joints into a global vector $\boldsymbol{d}$ and all the arriving wave vectors for all joints into $\boldsymbol{a}$, we obtain a global equation for the entire structure:

$$\boldsymbol{d}(\omega) = \boldsymbol{S}(\omega)\boldsymbol{a}(\omega) + \boldsymbol{s}(\omega) \tag{16}$$

or

$$\begin{Bmatrix} \boldsymbol{d}^1 \\ \boldsymbol{d}^2 \\ \vdots \\ \boldsymbol{d}^n \end{Bmatrix} = \begin{bmatrix} \boldsymbol{S}^1 & 0 & \cdots & 0 \\ 0 & \boldsymbol{S}^2 & \cdots & 0 \\ \vdots & \vdots & \vdots & \vdots \\ 0 & 0 & \cdots & \boldsymbol{S}^n \end{bmatrix} \begin{Bmatrix} \boldsymbol{a}^1 \\ \boldsymbol{a}^2 \\ \vdots \\ \boldsymbol{a}^n \end{Bmatrix} + \begin{Bmatrix} \boldsymbol{s}^1 \\ \boldsymbol{s}^2 \\ \vdots \\ \boldsymbol{s}^n \end{Bmatrix}$$

$\boldsymbol{S}$ is called the *global scattering matrix*, and $\boldsymbol{s}$ is called the *global source vector*. The size of the column matrix $\boldsymbol{d}$, $\boldsymbol{a}$, or $\boldsymbol{s}$ is $(2 \times 3m)$ because each member appears twice in the formulation of the global scatting matrix.

In the case of rigid frame or a structure with pinned joints, Eq. (16) contains two sets of unknowns, the departing wave vector $\boldsymbol{d}$ and the arriving wave vector $\boldsymbol{a}$ for all structure members. Another matrix equation that relates $\boldsymbol{d}$ and $\boldsymbol{a}$ is needed to determine either field vector in terms of the source vector $\boldsymbol{s}$.

B. Reverberation Matrix

Note that in a member JK the arriving wave vector $\boldsymbol{a}^{JK}$ to end J is also the departing wave vector $\boldsymbol{d}^{KJ}$ from the end K. The components of these two vectors, however, may be different in phase and sign:

$$a_j^{JK} = -e^{-ik_j l} d_j^{JK} \qquad (j = 1, 2, 3) \tag{17a}$$

Introducing the (3×3) phase matrix $\boldsymbol{P}^{JK}$ to account for this difference, we establish another set of equations for each member as follows:

$$\boldsymbol{a}^{JK} = \boldsymbol{P}^{JK}\boldsymbol{d}^{KJ} \tag{17b}$$

where

$$\boldsymbol{P}^{JK}(\boldsymbol{kl}) = \begin{bmatrix} -e^{-ik_1 l} & 0 & 0 \\ 0 & -e^{-ik_2 l} & 0 \\ 0 & 0 & -e^{-ik_3 l} \end{bmatrix}$$

Next $\boldsymbol{a}^{JK}$ is assembled into $\boldsymbol{a}^J$ and then into the global vector $\boldsymbol{a}$ in Eq. (16). The $\boldsymbol{d}^{KJ}$ vectors are similarly assembled. We designate the global vector for the assemblage of $\boldsymbol{d}^{KJ}$ by $\tilde{\boldsymbol{d}}$ because the sequence of components of $\tilde{\boldsymbol{d}}$ is different from that of $\boldsymbol{d}$, despite the fact that both contain the same departing field elements:

$$\boldsymbol{a} = \boldsymbol{P}\tilde{\boldsymbol{d}} \tag{18}$$

An element $\boldsymbol{d}^{JK}$ in the column matrix $\boldsymbol{d}$ appears also in the column matrix $\tilde{\boldsymbol{d}}$ but in a different position. The two identical elements, one in $\boldsymbol{d}$ and the other in $\tilde{\boldsymbol{d}}$, are related by the permutation matrix $\boldsymbol{U}$ as follows:

$$\tilde{\boldsymbol{d}} = \boldsymbol{U}\boldsymbol{d} \tag{19}$$

where $\boldsymbol{U}$ is a $6m \times 6m$ square matrix, of which each row and column consists of a single element of unity and the rest of the elements are zero. The precise form of $\boldsymbol{U}$ depends on the scheme by which neighboring joints are numbered and the sequence of assembling the $\boldsymbol{d}^J$ and $\boldsymbol{d}$. For example, if d_1^{25} and d_1^{52} occupy ith and pth elements, respectively, of the column matrix $\boldsymbol{d}$, then the elements U_{ip} and U_{pi} equal one, and the remaining elements in the ith row and pth column are zero.

From Eqs. (18) and (19) the second relationship between arriving wave vector $\boldsymbol{a}$ and departing wave vector $\boldsymbol{d}$ can be found as

$$\boldsymbol{a}(\omega) = \boldsymbol{P}(\boldsymbol{kl})\boldsymbol{U}\boldsymbol{d}(\omega) \tag{20}$$

This equation that relates $\boldsymbol{a}$ and $\boldsymbol{d}$ by the product of $\boldsymbol{PU}$ supplements Eq. (16) for solving $\boldsymbol{a}$ and $\boldsymbol{d}$ in terms of $\boldsymbol{s}$.

Substituting Eq. (20) into Eq. (16), we find

$$\boldsymbol{d} = \boldsymbol{SPU}\boldsymbol{d} + \boldsymbol{s} \tag{21}$$

which reduces to

$$\boldsymbol{d}(\omega) = [\boldsymbol{I} - \boldsymbol{R}(\boldsymbol{kl}, \omega)]^{-1}\boldsymbol{s}(\omega) \tag{22}$$

where $\boldsymbol{R}(\boldsymbol{kl}, \omega) = \boldsymbol{S}(\omega)\boldsymbol{P}(\boldsymbol{kl})\boldsymbol{U}$ is called a *reverberation matrix* for the structure. Once it is determined, then the departing wave vector $\boldsymbol{d}$ is obtained from Eq. (23), by first calculating the source vector $\boldsymbol{s}$ and then the inverse matrix of $[\boldsymbol{I} - \boldsymbol{R}]$. Thereupon from Eq. (20), we may calculate the arriving vector $\boldsymbol{a}$ for the entire structure.

IV. Steady-State Response and Transient Response of the Structure

A. Steady-State Responses

From Eqs. (6), (8), (9a), and (9b), we can calculate any physical quantities (displacement, force, moment, strain, etc.) in terms of the arriving vectors $\boldsymbol{a}$ and departing vectors $\boldsymbol{d}$ as discussed in the preceding section. Because we will compare the result of strains with experimental data, we calculate the extensional strain along the x axis due to the axial displacement by $\epsilon_u = \partial u/\partial x$ and due to lending by $\epsilon_v = c\partial^2 v_b/\partial x^2 (= \epsilon_{v2} + \epsilon_{v3})$, where c is the half-depth of the beam. Introducing two propagation matrices $\boldsymbol{A}_\epsilon(x)$ and $\boldsymbol{D}_\epsilon(x)$, we express the three parts of the extensional strain $(\epsilon_u, \epsilon_{v2}, \epsilon_{v3})$ in the form of a column matrix:

$$\hat{\boldsymbol{\epsilon}}^{JK}(x, \omega) = \boldsymbol{A}_\epsilon^{JK}(\boldsymbol{kx})\boldsymbol{a}^{JK}(\omega) + \boldsymbol{D}_\epsilon^{JK}(\boldsymbol{kx})\boldsymbol{d}^{JK}(\omega) \tag{23}$$

where $\boldsymbol{A}_\epsilon^{JK}$ and $\boldsymbol{D}_\epsilon^{JK}$ are given by

$$\boldsymbol{A}_\epsilon^{JK}(\boldsymbol{kx}) = \begin{bmatrix} ik_1 e^{ik_1 x} & 0 & 0 \\ 0 & -ck_2^2 e^{ik_2 x} & 0 \\ 0 & 0 & -ck_3^2 e^{ik_3 x} \end{bmatrix}$$

$$\boldsymbol{D}_\epsilon^{JK}(\boldsymbol{kx}) = \begin{bmatrix} -ik_1 e^{-ik_1 x} & 0 & 0 \\ 0 & -ck_2^2 e^{ik_2 x} & 0 \\ 0 & 0 & -ck_3^2 e^{-ik_3 x} \end{bmatrix}$$

Following the steps for stacking $\boldsymbol{a}$ and $\boldsymbol{d}$ and using Eqs. (20) and (22), we obtain the global strain matrix as

$$\hat{\boldsymbol{\epsilon}}(\boldsymbol{x}, \omega) = [\boldsymbol{A}_\epsilon(\boldsymbol{kx})\boldsymbol{P}(\boldsymbol{kl})\,\boldsymbol{U} + \boldsymbol{D}_\epsilon(\boldsymbol{kx})][\boldsymbol{I} - \boldsymbol{R}(\boldsymbol{kl}, \omega)]^{-1}\boldsymbol{s}(\omega) \tag{24}$$

Equation (24) is also the steady-state response in strains of the structure when the sources all have the common time factor $\exp(i\omega t)$. The oscillating strain $\hat{\epsilon}$ becomes infinitely large if the matrix $\boldsymbol{I} - \boldsymbol{R}$ is singular at certain frequencies or when the determinant of $\boldsymbol{I} - \boldsymbol{R}$ vanishes:

$$\det[\boldsymbol{I} - \boldsymbol{R}(\boldsymbol{kl}, \omega)] = 0 \tag{25}$$

The roots of this frequency equation $\omega = \omega_k$ $(k = 1, 2, \ldots, \infty)$ are the natural frequencies of the structure. This frequency equation is similar to that derived by Nagem and Williams,[7] based on the method of transfer matrix for these steady vectors (u, v_b, v_s, F, V, M) and standing-wave components in each member. In this paper we replaced the steady vector with the six components by the arriving wave vector $\boldsymbol{a}(a_1, a_2, a_3)$ and departing wave vector $\boldsymbol{d}(d_1, d_2, d_3)$ for traveling waves in each member. The evaluation of the Fourier-transformed extensional strains for the entire structure is now complete.

B. Transient Responses

For the transient response of the structures, the time-dependent strain $\epsilon(x, t)$ is determined from the inverse transform of $\hat{\epsilon}(x, \omega)$, according to Eq. (4b):

$$\epsilon(x, t) = \frac{1}{2\pi} \int_{-\infty}^{\infty} [\boldsymbol{A}_\epsilon \boldsymbol{P}\boldsymbol{U} + \boldsymbol{D}_\epsilon][\boldsymbol{I} - \boldsymbol{R}]^{-1} \boldsymbol{s} e^{i\omega t} \, d\omega \tag{26}$$

This integral has an infinite number of poles along the real axis of the complex ω plane, $\omega = \omega_k$, as determined by Eq. (25). Calculation of the roots for the natural frequency equation can be very difficult, as discussed in Ref. 7.

Following the methods of generalized ray, which sorts the reverberated waves in layer media into rays of waves,[12] we expand $[\boldsymbol{I} - \boldsymbol{R}]^{-1}$ into the Neumann series

$$[\boldsymbol{I} - \boldsymbol{R}]^{-1} = \boldsymbol{I} + \boldsymbol{R} + \boldsymbol{R}^2 + \cdots \boldsymbol{R}^m + \cdots$$

The integral is then reduced to

$$\epsilon(x, t) = \frac{1}{2\pi} \int_{-\infty}^{\infty} [\boldsymbol{A}_\epsilon \boldsymbol{P}\boldsymbol{U} + \boldsymbol{D}_\epsilon][\boldsymbol{I} + \boldsymbol{R} + \cdots + \boldsymbol{R}^m + \cdots] \boldsymbol{s} e^{i\omega t} \, d\omega \tag{27}$$

The poles at $\omega = \omega_k$ are thus removed from the integrand.

Note that the source vector $\hat{\boldsymbol{s}}(\omega)$ in either Eq. (26) or Eq. (27) contains the factor $\hat{f}(\omega)$, which is the Fourier transform of the time function $f(t)$ for an external force. The $\hat{f}(\omega)$ might introduce additional poles in the integral. In the ensuing numerical examples, we assume a single force with a unit step-time function $H(t)$ applied at joint 6:

$$f(t) = H(t) = \begin{cases} 1 & t > 0 \\ 0 & t < 0 \end{cases} \tag{28a}$$

The Fourier transform of $f(t)$ is $\hat{f}(\omega) = 1/(i\omega)$, which is singular at $\omega = 0$. This pole, however, is eliminated by the factors k_1, k_2, or k_3 and the propagation matrices $\boldsymbol{A}_\epsilon$ and $\boldsymbol{D}_\epsilon$.

Once the step response of the structure generated by a source with the step-time function is known, the transient response of the structure due to the arbitrary time function can be calculated from the Duhamel integral. Furthermore, the source with the step-time function generates waves in all members with a clearly defined wave front. As the time t approaches infinity, the time function for the source approaches unity, and the step response for the structure should approach the statical strain of the structure under a constant loading. This furnished a check on the calculations of dynamic response.

To determine the transient response, we must complete the inverse Fourier transform represented by either Eq. (26) or Eq. (27). As mentioned earlier, the integrand of Eq. (26) contains an infinite number of poles at $\omega = \omega_k$ ($k = 1, 2, \ldots, \infty$), where ω_k are real numbers for an elastic structure. In principle, the integral in Eq. (26) could be evaluated by summing the residues of the integrand at all poles, and so this is equivalent to evaluate accurately the contributions of all normal modes. The actual calculation, however, can be very difficult because numerical evaluation of the residues is very complicated, and only a finite number of poles can be located precisely.[7] To yield an accurate early time response, we need to include a large number of normal modes at high frequencies.

On the other hand, the integrand of Eq. (27) contains no poles other than those introduced by the source function. The integral can thus be evaluated numerically by applying the FFT algorithm. The application, however, is not routine because we desire to obtain the early time response (small t) as well as the long time response (large t).

C. Application of the FFT

Consider one element of the column matrix ϵ in Eq. (27) and express either the axial strain or bending strain at the local coordinate x of a structural member as follows:

$$\epsilon(t) = \frac{1}{2\pi} \int_{-\infty}^{\infty} \hat{f}(\omega) \hat{\epsilon}_D(\omega) \, e^{i\omega t} \, d\omega \tag{29a}$$

In this expression, the transform of the source time function $\hat{f}(\omega)$ has been separated from the source vector $\boldsymbol{s}$, and $\hat{\epsilon}_D(\omega)$ denotes the steady-state response under a single harmonic force. For numerical work we shall impose a cut of frequency $\pm\Omega$ on the upper and lower limit and reduce the infinite integral to a finite one. This cutoff frequency is possible if the time function in Eq. (28a) is bandwidth limited; therefore, we change $f(t)$ to a step-time function with finite duration t_a, that is,

$$f(t) = H(t) - H(t - t_a) \tag{28b}$$

The Fourier transform of this function is $\hat{f}(\omega) = (1 - e^{i\omega t_a})/(i\omega)$, and the bandwidth is $2\pi/t_a$. The cutoff frequency is thus selected as $\Omega = 2\pi/t_a$. For the original loading with a step-time function, the solution so obtained is valid only for $t < t_a$.

Dividing the bandwidth $(-\Omega, \Omega)$ into $2N$ equal intervals of frequency $\Delta\omega$ so that $N\Delta\omega = 2\Omega$, we reduce the integral in Eq. (29a) into a finite sum:

$$\epsilon(n\Delta t) = \frac{\Delta\omega}{2\pi} \sum_{k=-N+1}^{N} \hat{f}(k\Delta\omega) \hat{\epsilon}_D(k\Delta\omega) \, e^{ink\Delta\omega\Delta t} \tag{29b}$$

To apply the FFT algorithm for $\epsilon(t)$, we introduce the discrete Fourier inverse transform of $\hat{f}(\omega)\hat{\epsilon}_D(\omega)$ as

$$\epsilon[n] = \frac{1}{2N} \sum_{k=0}^{2N-1} \hat{f}[k] \hat{\epsilon}_D[k] \, e^{\frac{i\pi nk}{N}} \tag{30}$$

where $\hat{f}[k] = \hat{f}(k\Delta\omega)$ and $\hat{\epsilon}_D[k] = \hat{\epsilon}_D(k\Delta\omega)$ for $-N + 1 < k < N$ and both $\hat{f}[k]$ and $\hat{\epsilon}_D[k]$ are periodic series of $2N$. If $\Delta t \Delta\omega = \pi/N$, the $\epsilon[n]$ in Eq. (30) is equal to $\varepsilon(n\Delta t)$ times $\pi/(N\Delta\omega)$ in Eq. (29).

The assumption that $\hat{f}[k]\hat{\epsilon}_D[k]$ is periodic implies that $\varepsilon[n]$ is also periodic of period $2N$ or equivalent ($2N\Delta t \equiv T$) in the time domain. The question of how to represent $\pi/(N\Delta\omega)\epsilon(n\Delta t)$ accurately by $\varepsilon[n]$ is equivalent to how small the $\Delta\omega$ should be chosen or how large the period T should be.

The periodic function $\epsilon[n]$ is related to the exact (nonperiodic) answer $\epsilon(t)$ as follows:

$$\epsilon[n] - \frac{\pi}{\Omega}\epsilon(n\Delta t) = \frac{\pi}{\Omega} \sum_{j=-\infty, j\neq 0}^{\infty} \epsilon(n\Delta t + jN\Delta t) \tag{31}$$

Equation (31) shows that, if $\epsilon(t)$ is of significant size for $t > T$, the approximation $\epsilon[n]$ can be highly inaccurate because the response for $t > T$ will be aliased into the interval $0 < t < T$. Equation (30) will therefore be a good approximation to Eq. (29) if we know that $\epsilon(t)$ (the answer we desired) is insignificant for $t > T (= 2\pi/\Delta\omega)$.

D. Evaluation of the Inversion Transform by FFT

What we have discussed about the selections of Ω and T (or N) is common to all problems of inverse Fourier transforms by FFT.[13] The major advantage of working with the integral in Eq. (27) over that in Eq. (26) is in the physical contains of the respective integrands. As discussed in the previous paper,[8] the integrand in Eq. (27) contains the Neumann series expansion of $(\boldsymbol{I} - \boldsymbol{R})^{-1}$. The first term $\boldsymbol{I}$ represents waves being generated by the source at a joint; the second term $\boldsymbol{R}$ represents waves being reflected or transmitted once by the neighboring joints; and so on. Each term $\boldsymbol{R}^m$ in the series represents a set of waves arriving at the observational point, the latest one arriving at time $t = t_{\max}$. In the case of axial waves with constant speed c_1[8], $t_{\max}$ is estimated from the longest path along which the waves have been reverberated (scattered) m times by one or many joints. We thus select $T = t_a + t_{\max}$ and calculate the transient response only up to the time $t < t_a$.

When bending waves are involved as in the present case, there is no obvious choice for $t_{\max}$ because the wave is dispersive, and the wave speed approaches 0 at very low frequencies. However, a reasonable finite time interval t_b can still be estimated on the basis of the group velocity (less than c_1) for flexural waves. Once the t_b is chosen, we set $t'_{\max} = mt_b$, and the result from evaluating the inverse Fourier transform of the sum involving $(\boldsymbol{I} + \boldsymbol{R} + \cdots + \boldsymbol{R}^m)$ should die out for $t > t'_{\max} + t_a$. Returning to Eq. (31), if we chose $T = t'_{\max} + t_a$ and applied the FFT algorithm into Eq. (27), the aliasing error as defined in the right-hand side of the equation would be reduced to a minimum because the data $t > T$ would have little or no effect on the response.

In contrast, numerically taking the inverse transform of Eq. (25) can be quite complicated because it does not separate the response into sets of wave arrivals but instead represents the entire transient solution, which may be of quite a long duration.

V. Arrival Times of Synthesized Signals and Balance of Momenta at a Joint

In this section we show a typical numerical dynamic response of the truss shown in Fig. 1a for the purpose of checking the arrival times for the Fourier-synthesized signals and the balance of momenta. The sample truss shown in the Fig. 1a is taken from the laboratory model for a dynamic experiment,[10] and a detailed description of the model is given in the next section. The truss is composed of 17 square aluminum bars that are welded together at 10 joints, and it is supported by a hinge at joint 1 and a roller at joint 9. For numerical work all dimensions are normalized by the unit of length l_0, and the width of each panel is taken as $3l_0$. Hence, the length of each panel is 3 units, the height is 4 units, and the total span is 12 units. The unit of normalized time is $t_0 = l_0/c_1$, which is the time taken by the axial wave to travel the distance l_0. The product EA is taken as one unit of force f_0, and the external force applied at joint 6 is assumed to be one unit step function in this example.

A. Comparison with the Axial Waves Theories

In Ref. 8 we calculated the axial strains for each member of the truss shown in Fig. 1a on the basis of the theory of axial waves. The results for member 6-8 are shown in Fig. 2 for two cases: 1) considering only axial waves in the truss with rigid joints and 2) considering only axial waves in all structural members, revising the scattering coefficients at all joints to include the effect of bending waves. The result for case 1 is shown as short dashed lines and for case 2 as long dashed lines. In Fig. 2 results based on the general theory of this paper are shown as case 3 as a solid line.

The transient responses have been calculated with a FFT computer code for 90 t_0, using 30 terms in the series. The dynamic strain is seen to approach the static value of -0376 μm/m gradually. In case 3 we applied the complete scattering matrix in Eqs. (13) to determine all three components of a^{JK} and d^{JK} but omitted the second and third components of a^{JK} and d^{JK}. Case 1 in Ref. 8 considered only a_1^{JK} and d_1^{JK} in the evaluation of the scattering matrix.

Case 1 has been checked against another case calculated by a ray-tracing method in Ref. 9. As times increases, because the rays become too numerous, the ray-tracing method becomes impractical. Furthermore, ray tracing cannot be applied directly to the case involving bending waves because of the dispersion.

In Fig. 2 the first arrival of waves is seen clearly for all three cases, and this is expected because the axial waves are the fastest in all of the structural members. The arrival time of the synthesized signal by FFT agrees with that determined by the ray theory, the latter being the travel time of the axial wave from the note at joint 6 to the midpoint of member 6-8. Case 3 has shown additional dispersion because the theory allows for bending waves to be converted back into axial waves at all joints. Nevertheless, it is still possible to discern individual wave arrivals for cases 2 and 3 at earlier times before the initial waves have become too dispersed by multiple scatterings and because the axial wave response dominates at early times.

Comparisons of the axial strains in all three cases are also made for other members. The features are similar to those shown for the member 6-8. The axial wave theory (case 1) predicts the very early response well, but it diverges from the general theory of axial and flexural waves (case 3) very quickly as time increases. The results based on the revised axial wave theory (case 2) agree with those of case 3 over a much longer time, but the theory cannot predict strains generated by flexural waves, which are discussed in the next section.

B. Balance of Momenta at a Joint

In the general theory the linear momentum and angular momentum of a joint are balanced at all time, as stated in Eqs. (11). Although the matrices $a(\omega)$ and $d(\omega)$ for the steady-state response of the structure are calculated from Eqs. (11) together with Eqs. (12) and (20) for each value of ω, we must check whether the momenta of the transient response, which are determined from the inverse transform involving $a(\omega)$ and $d(\omega)$, are balanced at all times. Because we have neglected the masses of the joints [M^J in Eqs. (11)], balances of momenta are equivalent to the balance of forces and moments.

In Fig. 3 we plotted the axial forces in solid lines and shear forces in dashed lines in members 5-3, 5-4, 5-6, and 5-7, which are connected at joint 5, whereas a unit step compressive force $f_0 = EA$ is applied at joint 6. The forces shown in Fig. 3 are normalized by f_0, and the time is again normalized by t_0. The dynamic axial forces F^{JK} in four members differ from each other significantly, and the shear forces, although very small, also differ from each other. However, the sums for the X components and for the Y components of both axial and shear forces are nearly zero (to the order of 10^{-4}) and are depicted by a thick straight line along the time axis.

In Fig. 4 the moments in members 5-3, 5-4, 5-6, and 5-7 at joint 5 are plotted. All moments are normalized to $f_0 l_0$. The moments change rapidly from time to time, but their sum is nearly zero (to the order of 10^{-2}) for all time. The completeness of our theory and accuracy of the numerical evaluation are thus substantiated by this result.

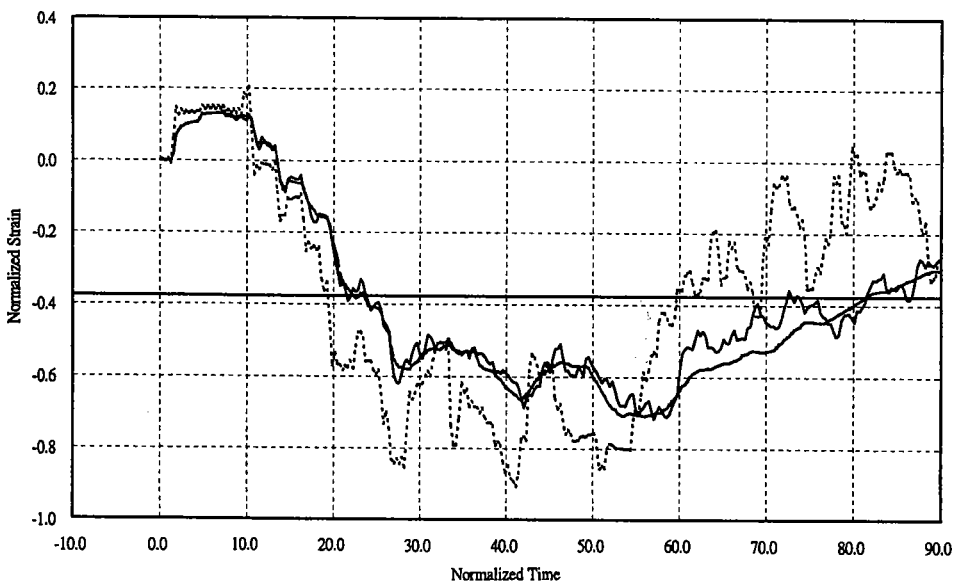

Fig. 2 Dynamic axial strain in member 6-8 based on three different theories: - - - -, case 1; — — —, case 2; and ——, case 3.

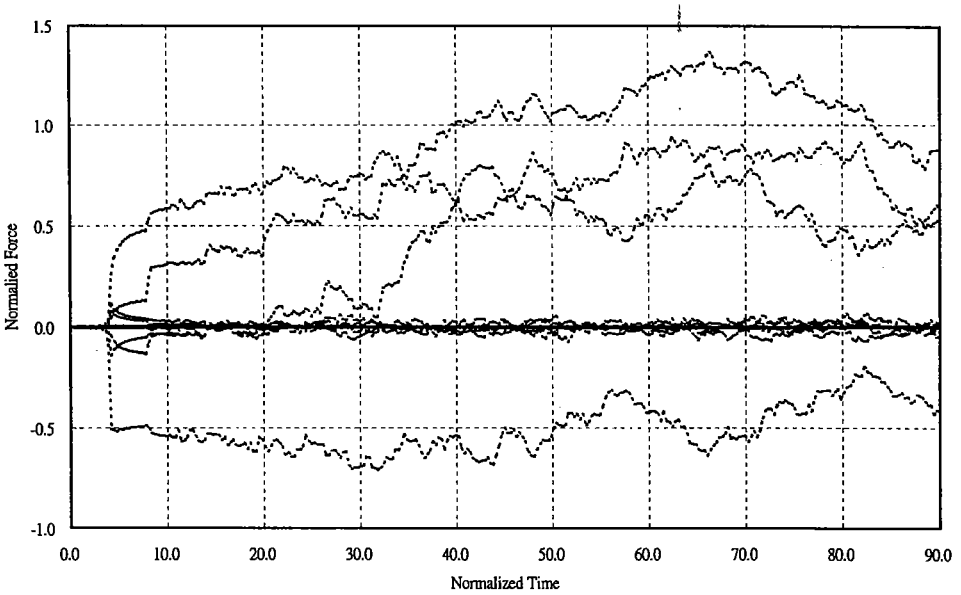

Fig. 3 Balances of forces at joint 5: ——, axial forces; - - - -, shear forces; and ▬, the sum of X components and Y components of all forces.

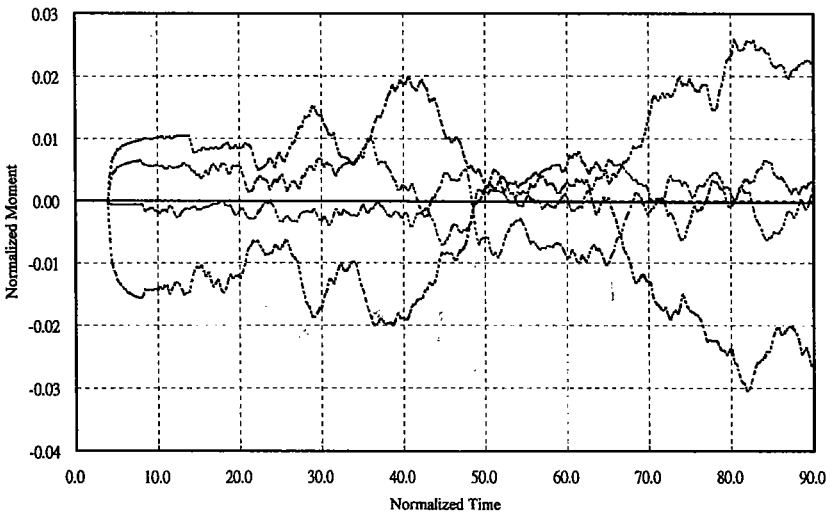

Fig. 4 Balances of moments at joint 5 (the sum of four moments being nearly zero).

VI. Axial and Bending Strains and Comparison with Experiments

Once the accuracy of the sample calculations was obtained, we calculated from Eq. (27) the axial and bending strains at the midpoints of all structural members and compared them with experimentally measured strains.[10] The axial strain is given by the first element of ϵ^{JK} for each member, and the bending strain equals the sum of the second and third elements. We shall hear only the theoretical and experimental results for three members, 5-7, 6-7, and 6-8, and the action of only one vertical force at joint 6.

A. Experiments

Experimental data were taken from a laboratory model developed for dynamic experiments described in Refs. 8 and 10. We deliberately chose asymmetrical configuration for the truss as shown in Fig. 1 to enhance the varieties of experimental data collections. The planar truss is composed of 17 square alumina rods that are welded to form four panels with 10 joints. The dimension for each panel is 12×16 in. or 0.305×0.406 m, and the span of the truss is 1.22 m. The cross-sectional area of the alumina rod is $\frac{1}{4} \times \frac{1}{4}$ in. or 4.03×10^{-3} m^2, and the material constants are $E = 69$ GPa and $G = 27$ GPa, respectively. Because we have assumed in the preceding section 3 units of length and so on for the width of the panel, the basic length unit is $l_0 = 0.102$ m, $t_0 = 20.2\ \mu$s, and $f_0 = EA = 2.782 \times 10^6$ N.

The model frame was actually suspended upside down at joints 1 and 9 to a heavy I beam with simulated hinge or roller support conditions, and the truss was preloaded by a heavy weight 113 N suspended by a fishing wire to joint 6. As mentioned in Ref. 8, the measured static strain for the rigid joint truss agreed closely with the theoretical values for a pin-connected truss. For instance, for the lower chord 4-6, vertical member 5-6, and upper chord 5-7, the measured strains ε in micrometers per meter (10^{-6}) and the theoretical values (given inside the parentheses) are, respectively, $\varepsilon_{46} = 32.0(30.6)$, $\varepsilon_{56} = 22.5(20.4)$, and $\varepsilon_{57} = -30.0(-30.6)$ when the weight of 113 N is suspended at joint 6. The corresponding experimental and theoretical values of axial strains (10^{-6}) because of bending are $\varepsilon_{46b} = 7.0(1.1)$, $\varepsilon_{56b} = 1.5(0.3)$, and $\varepsilon_{57b} = 0.0(1.1)$. The difference between the experimental and theoretical value for bending strain is much larger than that for the axial strain.

The dynamic loading is generated suddenly by burning the wire and releasing the weight. The condition of sudden unloading is simulated mathematically by the complementary Heaviside function $1 - H(t)$ for the theoretical model. The original data were then converted to those for the step loading [a unit Heaviside time function $H(t)$] by subtracting the experimental data for the step unloading from a constant value of the initial strain and static loading.

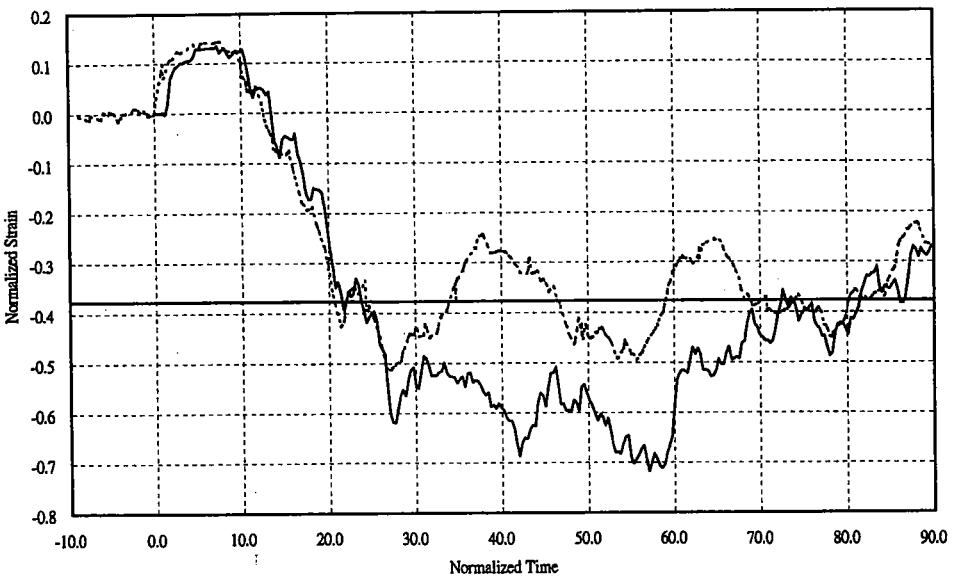

Fig. 5 Comparison of the theoretical values and experimental data for the axial strain in member 6-8: ——, theory, and · · · ·, experiment.

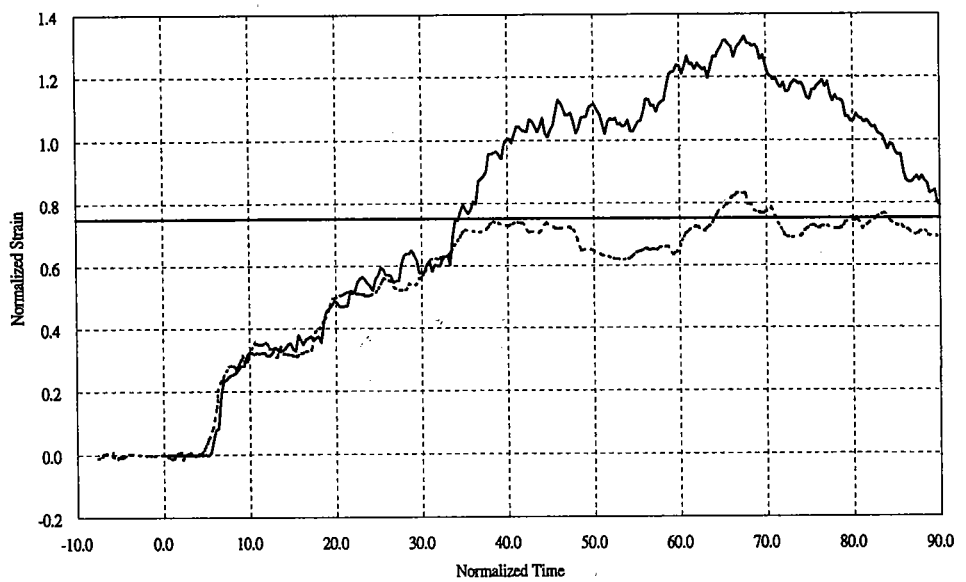

Fig. 6 Comparison of the theoretical value and experimental data for the axial strain in member 5-7: ——, theory, and · · · ·, experiment.

As shown in Fig. 1a, a unit compressive force $f_Y^6 = 113$ N in Eq. (11b) is suddenly applied to joint 6. The experimental static values of axial strains for respect members are shown in Figs. 5–7, and those of bending strain are shown in Figs. 8–10. In Figs. 5–7 the axial and bending strain are normalized to $\varepsilon_0 = f^6/EA = 40.6\ \mu$m/m, where f^6 equals the weight at joint 6, 113 N, and $EA = 2.782 \times 10^6$ N.

B. Axial Strains

Figures 5–7 show the axial strains in three members. The solid line is the result of the reverberation method from Eq. (27) (using 30 terms in the series expansion), and the dashed line is the experimental data. For the member 6-8 shown in Fig. 5, the theoretical and experimental results agree closely up until 30 t_0; the two results are close. After that the difference between theory and experiment increases. We believe that the discrepancy is caused by the oversimplifications of the mathematical model for the actual supports (a hinged and a roller), which is suggested by the observation that the discrepancy becomes large after about 30 t_0 and which is about equal to the time for all waves scattered twice at the supports.

Figures 6 and 7 show that the results compare for axial strains in members 5-7 and 6-7, respectively. As in Fig. 5, the theoretical results are very close until 30 t_0 have elapsed. Presumably, this is again caused by the supports.

In Figs. 5–7 we have indicated static values for the strains in each member. Both theoretical and experimental results gradually approach to the static value. There is considerable dynamic overshot in theoretical curves; the peak values bending 80% larger than static asymptotes in these members.

C. Bending Strains

In Figs. 8–10 we show the bending strains in three members of the truss. Again, the results based on Eq. (27) are shown by solid lines and the experimental data by dashed lines. Because the bending wave is slower than the axial wave, the bending signal starts later than the axial wave in all cases. Also, because of the dispersive nature of the wave, with higher frequencies faster than slower frequencies, the arrival starts with many small wavelets before the arrival of the main part of the signal.

Figure 8 is for member 6-8. The experiment and theory diverge again at around 30 t_0. Figures 9 and 10 show the bending strain in members 5-7 and 6-7, respectively. Figures 9 and 10 exhibit features similar to those of Fig. 8, and the divergences starts around 30 t_0.

From these figures we find from the magnitude of the maximum bending strain that the chord members 5-7 and 6-8 are twice as large

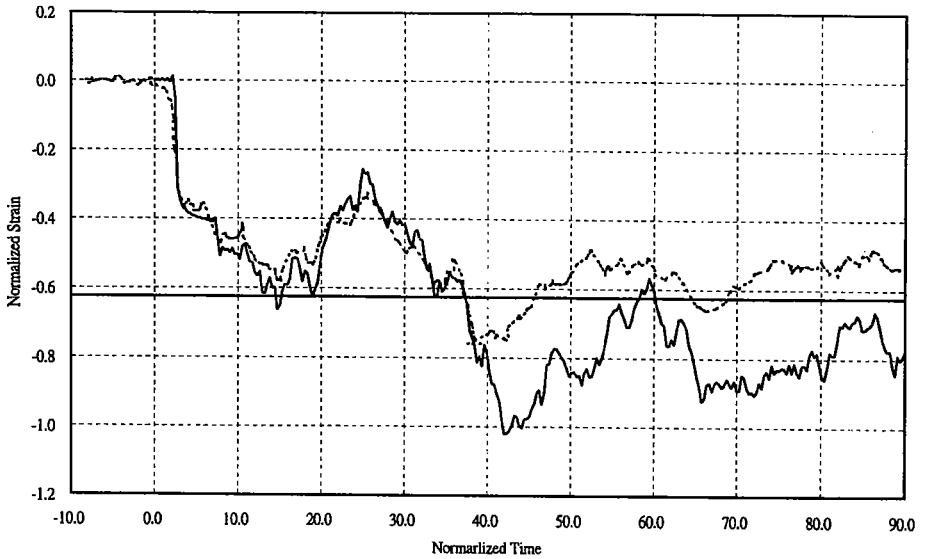

Fig. 7 Comparison of the theoretical value and experimental data for the axial strain in member 6-7: ——, theory, and · · · ·, experiment.

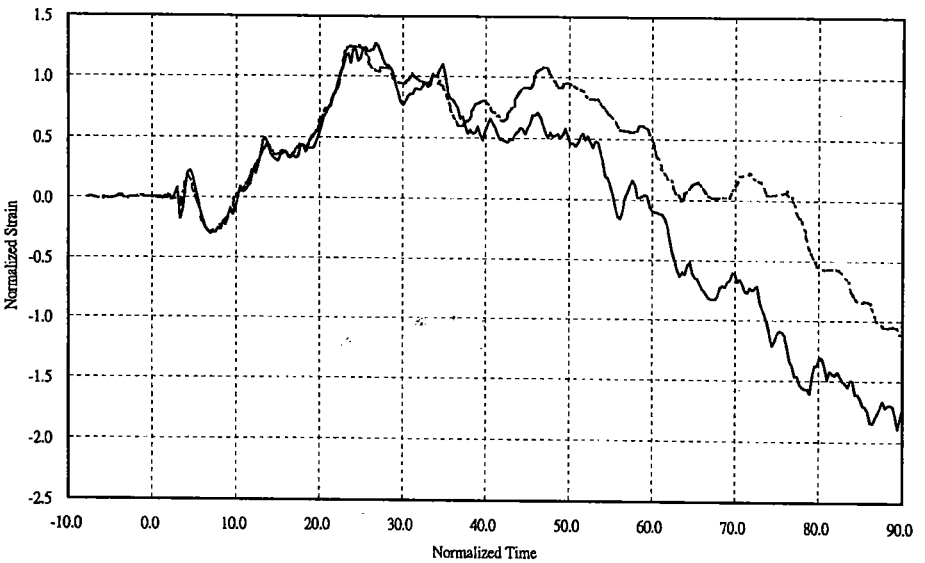

Fig. 8 Comparison of the theoretical value and experimental data for the bending strain in member 6-8: ——, theory, and · · · ·, experiment.

Fig. 9 Comparison of the theoretical value and experimental data for the bending strain in member 5-7: ——, theory, and · · · ·, experiment.

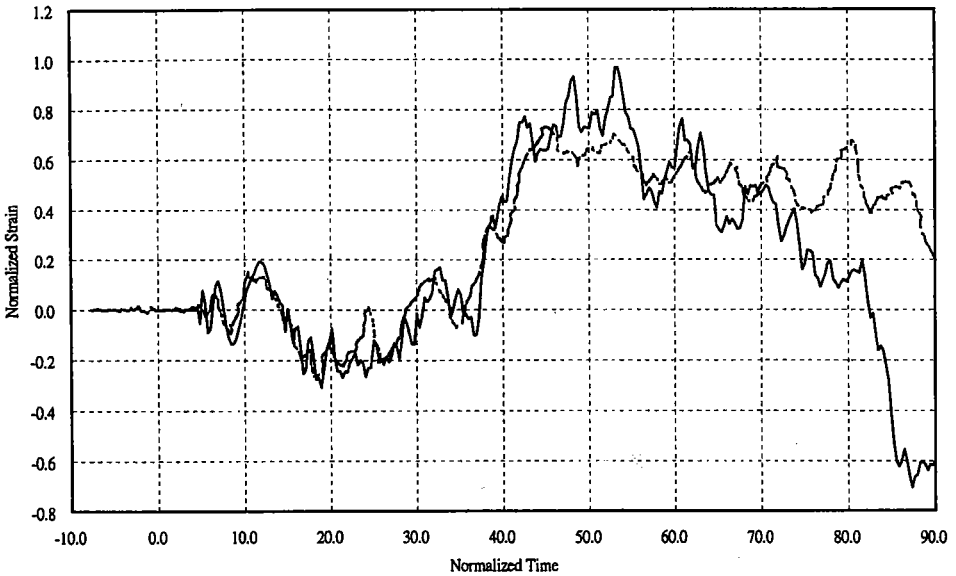

Fig. 10 Comparison of the theoretical value and experimental data for the bending strain in member 6-7: ——, theory, and · · · ·, experiment.

as the diagonal member 6-7. The magnitudes of bending strains in all members, however, are of the same order as those of axial strains shown in the preceding three figures. The static values for bending strains are not shown in Figs. 8–10 because they are supposed to be zero for a truss with pined joints. Even for the truss with rigid joints, the static values are still very small for the model used in the experiment.[14] We do not have an explanation for the very large bending strains in the truss and dynamic loading as shown in Fig. 10.

VII. Conclusion

We have presented a new matrix formulation for analyzing the dynamic response and propagation of elastic waves in a structure that is composed of beams and rods and connected by a rigid or pinned joint. The formulation, which is named as the method of reverberation matrix, is similar to that proposed by Negam and Williams[7] for steady-state waves. Their method showed higher accuracy than the existing dynamic stiffness method or finite element method in the evaluation of the natural frequencies of framed structures.

The major advantage of the method of the reverberation matrix lies in the determining of transient responses of structures. Combined with a refined FFT algorithm, the method yields accurate arrival time and initial responses for all three modes of waves (axial wave and two modes of flexural waves), as well as correct asymptotic values (static values) for long time responses. The completeness and accuracy of this formulation is further demonstrated by the balance of linear and angular momenta at the joint, as shown in Figs. 3 and 4 for all time. The key step in the analysis is the conversion of $(\boldsymbol{I}-\boldsymbol{R})^{-1}$ to a power series of $\boldsymbol{I}$ as shown in Eq. (27).

Comparing with a set of carefully conducted experimental data for a model truss, we found that the theoretical results agree closely with the experimental data at early times. However, they differ around $t=30\,t_0$, which is estimated as the time required for the waves traveling through the support twice, or traveling around the entire truss once, and so this indicates that the mathematical condition for the hinged and roller support of the truss should be reexamined. The rather large dynamic overshot over the static values shown in Figs. 5–7 after $t>30\,t_0$ should be examined concurrently.

Hopefully, the method of the reverberation matrix can be applied to determine rationally the impact factor, which is the ratio of the maximum dynamic response to the static response, for truss-type structures. Aside from precise dynamic stress analysis, the detailed and accurate evaluation of dynamic response history will be useful for system identification and for active control of the structures.

Acknowledgments

This research was supported first by the Office of Naval Research through a grant to Cornell University in 1987–1989 and later by the National Science Council, China, through a grant to National Taiwan University in 1994–1995. Their support and assistance are gratefully acknowledged. The manuscript was extensively revised by the first author during his visitation to the Southeast University at Nanjing in the Spring of 1998. He acknowledges the hospitality of the university and the able assistance of Jian-Ming Hua of Southeast University.

References

[1]Pestel, E. C., and Leckie, F. A., *Matrix Methods in Elastomechanics*, McGraw–Hill, New York, 1963, Chap. 10.

[2]Clough, R. W., and Penzin, J., *Dynamics of Structures*, McGraw–Hill, New York, 1975, Chap. 4.

[3]Berger, B. S., and Shore, S., "Dynamic Response of Lattice-Type Structures," *Journal of the Engineering Mechanics*, Vol. 89, No. EM2, 1963, pp. 47–70.

[4]Uhrig, R., "The Transfer Matrix Method Seen as One Method of Structural Analysis Among Others," *Journal of Sound and Vibrations*, Vol. 4, No. 1, 1966, pp. 136–148.

[5]Doyle, J. F., and Kamle, S., "Wave Propagation in Structure," Springer–Verlag, New York, 1989, Chap. 5.

[6]Bathe, K. J., and Wilson, E. L., *Numerical Methods in Finite Element Analysis*, Prentice–Hall, Englewood Cliffs, NJ, 1976, Chap. 10.

[7]Nagem, R. J., and Williams, J. H., "Dynamic Analysis of Large Space Structure Using Transfer Matrices and Joint Coupling Matrices," *Mechanical Structure and Machine*, Vol. 17, No. 3, 1989, pp. 349–371.

[8]Howard, S. M., and Pao, Y.-H., "Analysis and Experiments on Stress Waves in Planar Trusses," *Journal of Engineering Mechanics*, Vol. 124, No. 8, 1998, pp. 884–891.

[9]Boley, B. A., and Chao, C. C., "Impact on Pin-Jointed Trusses," *American Society of Civil Engineers Transactions*, Vol. 122, No. 1, 1957, pp. 39–63.

[10]Howard, S. M., "Transient Stress Waves in Trusses and Frames," Ph.D. Dissertation, Dept. of Theoretical and Applied Mechanics, Cornell Univ., Ithaca, NY, Jan. 1990.

[11]Timoshenko, S., *Vibration Problems in Engineering*, 3rd ed., Van Nostrand Co., New York, 1955, Chap. 5.

[12]Gopalakrishnan, S., Martin, M., and Doyle, J. F., "A Matrix Methodology for Spectral Analysis of Wave Propagation in Multiple Connected Timoshenko Beams," *Journal of Sound and Vibration*, Vol. 158, No. 1, 1992, pp. 11–24.

[13]Yong, Y., and Lin, Y. K., "Dynamics of Complex Truss-Type Space Structures," *AIAA Journal*, Vol. 28, No. 7, 1990, pp. 1250–1258.

[14]Oppenheim, A. V., *Discrete-Time Signal Processing*, Prentice–Hall, Englewood Cliffs, NJ, 1989.

R. K. Kapania
Associate Editor